

Sorption Paper Title

Jonathan G. V. Ström^a, Shuai Xie^a, Eric M. Suuberg^a

These authors contributed equally to this work

^a*Brown University, School of Engineering, Providence, RI, USA*

Abstract

Abstract here

Keywords: Vapor intrusion, Temporal variability, Sorption, Attenuation factor

1. Introduction

Many vapor intrusion (VI) contaminants has the capacity to sorb onto soil and various common indoor materials, but the role and more importantly, the consequences of these sorption processes in VI are poorly understood[1, 2?]. The migration of contaminant vapors from its source into the VI affected building and potential indoor sources are usually the prime concern in VI investigations. Rarely is the sorbed contaminant vapors in the soil or indoor considered in an investigation, but these may potentially act as a capacitor, storing and releasing contaminant vapors in response to a change in contaminant concentration. Consequently, contaminant vapors may be much more persistent at a site that has undergone remediation, potentially reducing the effectiveness of mitigation systems, or impeding site investigations.

It is well recognized that building materials has the capacity that sorb pollutants. The sorptive capacity of various volatile organic compounds (VOCs) of concern in VI have been tested on a variety of building materials, such as density board[?], gypsum wallboard[?], and plywood and carpets[?]. However, most of these studies used relative high contaminant concentrations, usually around mg/m^3 [?] or even higher. This is several magnitudes higher than the concentrations relevant in VI and due to the non-linear nature of sorption with respect to concentration, sorption studies at lower concentration are needed.

Email address: `eric_suuberg@brown.edu` (Eric M. Suuberg)

Most of the VOC sorption studies have also focused on the interaction between building materials and formaldehyde[?], toluene, and decane[?]. However, one of the contaminants of greatest concern in VI - trichloroethylene (TCE), has not received likewise attention. This is despite the fact that sorbing TCE (and other VOCs) on activated carbon is extensively used to treat indoor air contaminant and their use with passive sorption tube samplers[3].

Over the years many VI sites have been investigated for their potential exposure risk. Most of these are conducted by private industries but a few notable academic ventures exist as well. Two well-known examples of these are the studies of "Sun Devil Manor" near Hill Air Force Base in Utah, and a building in Indianapolis, Indiana. Both of these sites were outfitted with a wide variety of instrumentation to investigate the VI drivers at these sites. These studies yielded some of the richest VI datasets available and gave invaluable insights, in particular in the application of CPM[4] and sub-slab depressurization (SSD) mitigation systems[5, 6]. However, neither of these studies considered the role of sorption had at these sites.

The potential impact of sorption may perhaps be most significant in the application of the controlled pressure method and various mitigation schemes. The controlled pressure method (CPM) is the forced over- and depressurization of a building to max- and minimize the contaminant entry to the building. This aids the investigator to ascertain the worst-case VI scenario and help identify potential indoor contaminant sources[7, 4]. However, if the building has a large capacity to sorb contaminant vapors onto various materials, these may be sorbed and desorbed in response to the changing condition, potentially preventing corresponding changes in indoor air contaminant concentrations. The same is true for various mitigation schemes, while they may successfully prevent contaminant vapors from entering the house, these may still be released from the interior over an unknown period of time[1, 2].

In the past VI models have been used to gain insight into VI when no field or experimental data has been available. Previously examples of VI modeling studies are the role of rainfall in VI[8], or drivers of temporal variability in some of the aforementioned sites[9]. However, while many VI models include a sorption term in the governing equation for contaminant transport in soils, none have explored the role of sorption in VI in a transient simulation. The reason for this is two-fold. First, there has been a general lack of interest in sorption and VI thus far. Secondly, the vast majority of VI modeling efforts

67 and studies has focused on steady-state analyses of VI, and sorption only
68 affects soil contaminant transport in time-dependent scenarios.

69 To bridge this knowledge gap we will begin to explore the role of sorp-
70 tion in VI through a combined effort of experimental and simulation work.
71 Sorption data of TCE on various common indoor materials and Applying soil
72 will be measured in a fixed bed sorption experiment. These sorption data
73 will then be incorporated into a three-dimensional finite element model of
74 VI. For this purpose we will consider a prototypical VI scenario where a free-
75 standing house with a basement is overlying a homogenously contaminated
76 groundwater source. Using this model we will investigate how the dynamic
77 contaminant transport is affected in general by sorption, how indoor sorp-
78 tion materials affect indoor air concentration as the building's pressurization
79 fluctuates and how indoor air concentration are affected by indoor materials
80 following successful mitigation of the structure.

81 2. Methods

82 2.1. Experimental Setup

83 The TCE dynamic sorption process of different building materials were
84 determined by use of a method schematically shown in Figure 1. This method
85 involved a selected material contained in an adsorption column through which
86 TCE-containing gas was passed, and subsequent thermal desorption and mea-
87 surement of the total amount of adsorption. During the adsorption part of
88 the process, stainless steel tubes were packed with building materials held in
89 place by glass wool. The amount of building material normally held in the
90 tube was around 1 g. It was determined that neither the glass wool nor the
91 stainless steel tube would retain significant amounts of TCE. The sample-
92 containing tubes were first exposed desired low concentrations of TCE in
93 nitrogen, which were then allowed to interact with the flow for varying pe-
94 riods of time. The typical flow rate of the nitrogen was 60 ml/min and the
95 concentrations of TCE was around 1.1 ppbv. All of these adsorption experi-
96 ments were conducted at room temperature. After a given time of exposure
97 to the TCE-containing flow, that flow was stopped, and the sample tube
98 was attached to a sorbent tube placed downstream of the sample tube. The
99 sample tube was arranged such that the direction of the nitrogen flow in
100 the subsequent desorption process was opposite that of the TCE-containing
101 nitrogen flow during the adsorption process. During the thermal desorption

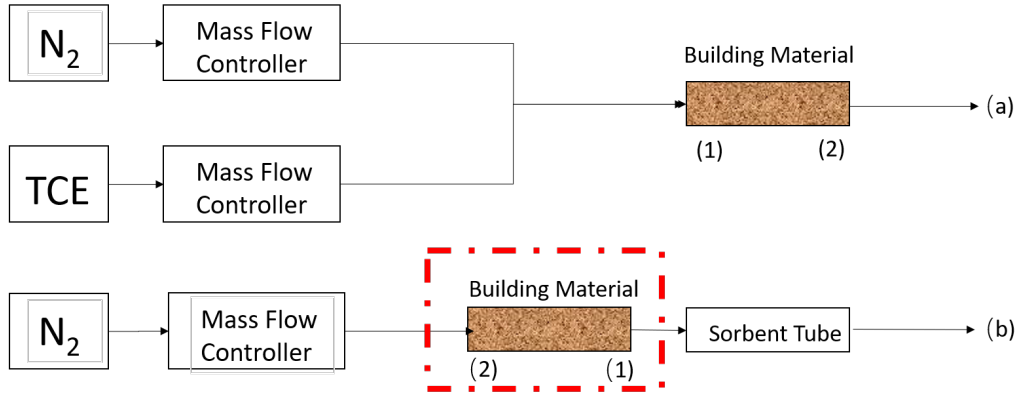


Figure 1: Schematic of experimental setup.

step, the sample containing tube was covered by a heating mantle which permitted its heating at 100 °C. This allowed fully desorbing the TCE which had been held on the sample into a pure nitrogen flow, which carried it to the room temperature downstream sorbent tube, where it was again fully adsorbed. These tubes fully capture all of the TCE desorbed, from the samples, and the amount of TCE was analyzed by Gas Chromatography (GC) with an Electron Capture Detector(ECD).

2.2. Numerical Model

To investigate the role of sorption in VI, we consider a simple VI scenario. Here we consider a house with a 10 by 10 m footprint, with the foundation bottom located 1 m below ground surface (bgs). The sole contaminant source is an uniformly TCE contaminated groundwater located 4 bgs, and the soil surrounding the house is assumed to homogenous and of a singular type. All contaminant vapors are assumed to enter the house through breaches in the foundation, modeled as a 1 cm wide crack that runs along the perimeter of the house. Finally we assume that sorption processes can occur both in the soil matrix and in the indoor environment (on various indoor materials).

Modeling this scenario requires us to simulate a couple of physics, many of which depend and interact with each other. The governing equations and the physics they govern are:

1. van Genuchten retention model - soil moisture.
2. Darcy's Law - air flow in the porous media.
3. Transport equation - contaminant transport in porous media.

Figure 2: The vapor intrusion model

125 4. Continuously stirred tank reactor (CSTR) - contaminant concentration
126 in the indoor environment.

127 These physics are implemented in COMSOL Multiphysics, a commercial
128 finite-element method package, which is used to solve our model. It is impor-
129 tant to note that the indoor environment is implicitly modeled, but instead
130 only given by the CSTR equation; the soil domain is explicitly modeled.

131 2.2.1. Vadose Zone Moisture Content

132 Since the contaminant transport occurs through three-phased the vadose
133 zone, it is important that we correctly account for soil moisture content and
134 its effect on advective and diffusive transport. In this modeled scenario, we
135 assume that the soil moisture is at steady-state and does not change, and
136 thus the soil moisture content is given by the retention model developed by
137 van Genuchten.

The van Genuchten retention model gives the soil water saturation as a function of elevation above groundwater. In turn this gives the water and gas filled porosities, and the relative permeability of the soil matrix.

$$Se = \begin{cases} \frac{1}{(1+\alpha z^n)^m} & z < 0 \\ 1 & z \geq 0 \end{cases} \quad (1)$$

$$\theta_w = \begin{cases} \theta_r + Se(\theta_s - \theta_r) & z < 0 \\ \theta_s & z \geq 0 \end{cases} \quad (2)$$

$$k_r = \begin{cases} Se^l [1 - (1 - Se^{\frac{1}{m}})]^2 & z < 0 \\ 0 & z \geq 0 \end{cases} \quad (3)$$

138 Se is the saturation, and ranges from 0 to 1, which represent completely un-
139 to fully saturated; z is the elevation above the groundwater in meters; θ_r ,
140 θ_s , θ_w , and θ_g are the residual moisture content, saturated porosity (or just
141 porosity), and water and air filled porosities respectively. All units are in
142 volume of phase divided by the volume of soil; k_r is the relative permeability
143 of water, which modifies the saturated permeability. This too ranges from 0
144 to 1, indicating completely im- and permeable respectively. $1 - k_r$ gives the
145 relative permeability of air.

146 *2.2.2. Gas Flow In The Vadose Zone*

147 The gas flow in the vadose zone is governed by a modified version of
 148 Darcy's Law. Originally, Darcy's Law was developed to describe flow in
 149 saturated porous media, but since we're interested in flow in unsaturated
 150 media, modification is necessary. An effective permeability that depends
 151 on the relative permeability from van Genuchten is introduced to allow for
 152 correct flow profiles in unsaturated porous media.

153 The vapor flow governing equation is given by

$$\frac{\partial}{\partial t}(\rho\theta_s) + \nabla \cdot \rho \left(- \frac{(1 - k_r)\kappa}{\mu} \nabla p \right) = 0 \quad (4)$$

154 Here ρ is the fluid density; ∇ is the del operator; κ is the saturated per-
 155 meability; μ is the fluid viscosity; and p is the fluid pressure. We assume
 156 that the contaminant vapors are so dilute that the gas flow properties can
 157 be taken to be those of air, and specifically at 20 °C and all the transport
 158 properties may be found in Table 1.

Boundary Conditions. To solve (4) we assign the atmosphere boundary (see
 Figure 2) to be at reference pressure and act as a gauge, i.e. zero pressure.
 The foundation crack boundary is assigned the indoor-outdoor pressure dif-
 ference value. Remaining boundaries are no-flow boundary conditions.

Atmosphere	$p = 0$ (Pa)	(5)
------------	--------------	-----

Foundation crack	$p = p_{\text{in/out}}$ (Pa)	(6)
------------------	------------------------------	-----

All other	$-\vec{n} \cdot \rho_{\text{air}} \vec{u} = 0$ (kg/(m ² · s))	(7)
-----------	--	-----

159 Here \vec{n} and \vec{u} are the boundary normal and gas velocity vectors.

160 *Initial Conditions.* For steady-state problems, the initial conditions don't
 161 matter, but is simply zero for the entire domain. When solving transient,
 162 the initial conditions are given by the steady-state solution.

163 *2.2.3. Mass Transport In The Vadose Zone*

164 Contaminants in the vadose zone exist in three phases - gaseous, solved in
 165 water, and sorbed onto soil particles. While there are three distinct phases,
 166 the water and gas phases are related via Henry's Law (8).

$$c_g = K_H c_w \quad (8)$$

167 Where c_g and c_w are the gas and water phase concentrations respectively in
 168 mol/m³; K_H is the dimensionless Henry's Law constant.

169 In this work, we consider sorption between the soil and vapor phases, as
 170 a function of the water contaminant concentration, through linear sorption
 171 (9).

$$c_s = K_{\text{ads}} \rho_b c_g = K_{\text{ads}} \frac{\rho}{1 - \theta_t} K_H c_w \quad (9)$$

172 Here the c_s is the solid phase concentration in mol/kg; ρ_b is the bulk density
 173 of the soil kg/m³, which is given by the density ρ and the total soil porosity
 174 θ_t ; K_{ads} is the sorption isotherm in m³/kg. Using Henry's Law and the linear
 175 isotherm we can express the total contaminant concentration in terms of the
 176 water contaminant concentration.

177 Mass transport in the vadose zone is governed by diffusion and advection
 178 and is given by (10).

$$R \frac{\partial c}{\partial t} = \nabla \cdot [D_{\text{eff}} \nabla c] - K_H \vec{u} \cdot \nabla c \quad (10)$$

179 The first term in (10) gives the change in contaminant water concentration
 180 with respect to time, modified by the *retardation factor*, R , which is discussed
 181 below; The second is the effective diffusive flux which is modified by the
 182 effective diffusion coefficient D_{eff} which is also discussed below. The third is
 183 the advective flux where \vec{u} is the soil-gas velocity from Darcy's Law, which
 184 when multiplied with K_H gives the gas phase concentration advective flux.

185 *Contaminant entry into the building.* The contaminant enters the building
 186 through a combination of advection and diffusive fluxes and is given by (11).

$$j_{ck} = \begin{cases} u_{ck} c_g - \frac{D_{\text{air}}}{L_{\text{slab}}} (c_{in} - c_g) & u_{ck} \geq 0 \\ u_{ck} c_{in} - \frac{D_{\text{air}}}{L_{\text{slab}}} (c_{in} - c_g) & u_{ck} < 0 \end{cases} \quad (11)$$

187 Here the j_{ck} is the molar contaminant flux into the building in mol/(m² · s);
 188 D_{air} is the contaminant diffusion coefficient in pure air in m²/s; L_{slab} is the
 189 thickness of the foundation slab in m. The flux expression changes if there
 190 is a bulk flow into the building, i.e. $u_{ck} \geq 0$, or out of the building.

191 *Retardation factor.* As the contaminants are transported through the vadose
 192 zone, the partitioning between the various phases increases the contaminant

193 residency time, retarding the transport of contaminants. This effect is rep-
 194 resented by R which is the retardation factor (12).

$$R = \theta_w + \theta_g K_H + \rho_b K_H K_{\text{ads}} \quad (12)$$

Here θ_w , θ_g are the water and gas filled soil porosities; K_{ads} is the solid-gas phase sorption isotherm in m^3/kg . The diffusive and advective transport retardation is proportional to the inverse of R .

$$D_{\text{retarded}} = \frac{D_{\text{eff}}}{R} \quad (13)$$

$$\vec{u}_{\text{retarded}} = \frac{\vec{u}}{R} \quad (14)$$

195 It should be noted that the soil-gas velocity, \vec{u} , is not retarded in of itself,
 196 but rather just the contaminant being transported through advection, giving
 197 a effective bulk velocity.

198 *Effective diffusivity.* The effective diffusivity in the vadose zone varies with
 199 the soil moisture content, from being close to that in water when fully sat-
 200 urated and vice versa. Millington-Quirk developed (15) which describes the
 201 effective diffusivity in variably saturated porous media.

$$D_{\text{eff}} = D_{\text{water}} \frac{\theta_w^{\frac{7}{3}}}{\theta_t^2} + \frac{D_{\text{air}}}{K_H} \frac{\theta_g^{\frac{7}{3}}}{\theta_t^2} \quad (15)$$

202 Where the porosity fractions are the water and gas phase tortuosity terms;
 203 D_{air} and D_{water} are the contaminant diffusion coefficient in air and water
 204 respectively in m^2/s .

Boundary Conditions. A few boundary conditions are required to solve (10). In this model, the sole contaminant source is assumed to be the homogenously contaminated groundwater, which we assume to have a fixed concentration. The atmosphere acts as a contaminant sink, and any contaminant that makes it to this boundary is infinitely diluted, thus this is simply a zero concentration boundary condition. Contaminants leave the soil domain and enter the building through a combination of advective and diffusive gas phase transport. The last boundary condition is applied to all other boundaries and is

a no-flow boundary.

$$\text{Groundwater} \quad c_w = 0 \text{ (mol/m}^3\text{)} \quad (16)$$

$$\text{Atmosphere} \quad c_w = c_{gw} \text{ (mol/m}^3\text{)} \quad (17)$$

$$\text{Foundation crack} \quad -\vec{n} \cdot \vec{N} = -\frac{j_{ck}}{K_H} \text{ (mol/(m}^2 \cdot \text{s))} \quad (18)$$

$$\text{All other} \quad -\vec{n} \cdot \vec{N} = 0 \text{ (mol/(m}^2 \cdot \text{s))} \quad (19)$$

$\vec{n} \cdot \vec{N}$ is the dot product between the boundary normal vector and the contaminant flux; j_{ck} is the contaminant vapor flux into the building. We assume that only contaminants in the gas phase enter the building, and dividing j_{ck} by K_H we get proper accounting in terms of the water phase concentration.

Initial Conditions. For a steady-state condition the initial conditions don't matter, but are set to be zero everywhere. For transient simulations in this work, the steady-state solution is always used as an initial condition.

2.2.4. Indoor Environment

The indoor air space is modeled as a continuously stirred tank reactor (CSTR) given by (20). Contaminants are assumed to only enter through the foundation crack, represented by n_{ck} , which is calculated by integrating the contaminant flux over the foundation crack boundary. The product of air exchange rate, which govern how many house volumes are exchanged with the outside per time unit, and indoor air contaminant concentration gives the contaminant exit rate. The sorption of contaminant is given by the sorption reaction term in (22) and the sorbed contaminant concentration is given by (21).

$$V_{\text{bldg}} \frac{\partial c_{\text{in}}}{\partial t} = n_{\text{ck}} - A_e c_{\text{in}} V_{\text{bldg}} + r_{\text{sorb}} V_{\text{mat}} \quad (20)$$

$$V_{\text{mat}} \frac{\partial c_{\text{sorb}}}{\partial t} = -r_{\text{sorb}} V_{\text{mat}} \quad (21)$$

$$r_{\text{sorb}} = k_1 c_{\text{sorb}} - k_2 c_{\text{in}} \quad (22)$$

$$n_{\text{ck}} = \int_{A_{ck}} j_{ck} dA \quad (23)$$

Here V_{bldg} and V_{mat} are the indoor control volume and volume of indoor material in m^3 ; c_{in} and c_{sorb} are the indoor and sorbed (onto the indoor

Table 1: Transport properties and model parameters

material) contaminant concentrations in mol/m^3 ; n_{entry} is the contaminant entry rate in mol/s , which is calculated by integrating the contaminant flux j_{ck} over the foundation crack area; r_{sorb} sorption rate in $\text{mol}/(\text{m}^3 \cdot \text{s})$; k_1 and k_2 are desorption and sorption reaction constants in $1/\text{s}$.

Fitting Kinetic Parameters. To calculate the indoor sorption rate we need k_1 and k_2 . These values are found by solving (22) numerically and then finding the best k_1 and k_2 by fitting them to the experimental data via least square. We use Runge-Kutta method of order 5(4) as the numerical solve, which is implemented together with the least square method in the SciPy python package[10].

3. Results & Discussion

3.1. Fitting Sorption Parameters

Using the numerical fitting scheme described in section 2.2.4 with the sorption data from the method described in section 2.1, the kinetic sorption parameters k_1 and k_2 are fitted. Figure 3 shows the result of this fitting and the sorption data for three select materials - wood, Appling soil, and cinderblock concrete. The k_1 and k_2 represent the rate at which TCE desorbs and sorbs respectively onto/from the material of interest. The equilibrium sorption constant is, using the formulation in (22), given by

$$K = \frac{k_1}{k_2} \quad (24)$$

and is used as the sorption isotherm. Here a small K indicate that there is a greater propensity for contaminant sorption.

To use the soil sorption isotherm in (10) K needs to be converted from being unitless to m^3/kg . This is done by multiplying the inverse of K isotherm with inverse of the soil bulk density ρ_b , which is taken to be $1460 \text{ kg}/\text{m}^3$.

$$K_{\text{ads}} = \frac{1}{K\rho_b} = 5.28 \text{ (m}^3/\text{kg)} \quad (25)$$

Table 2 shows the fitted parameters for the tested materials. Based on this these results we can see that cinderblock and soil have orders of magnitude

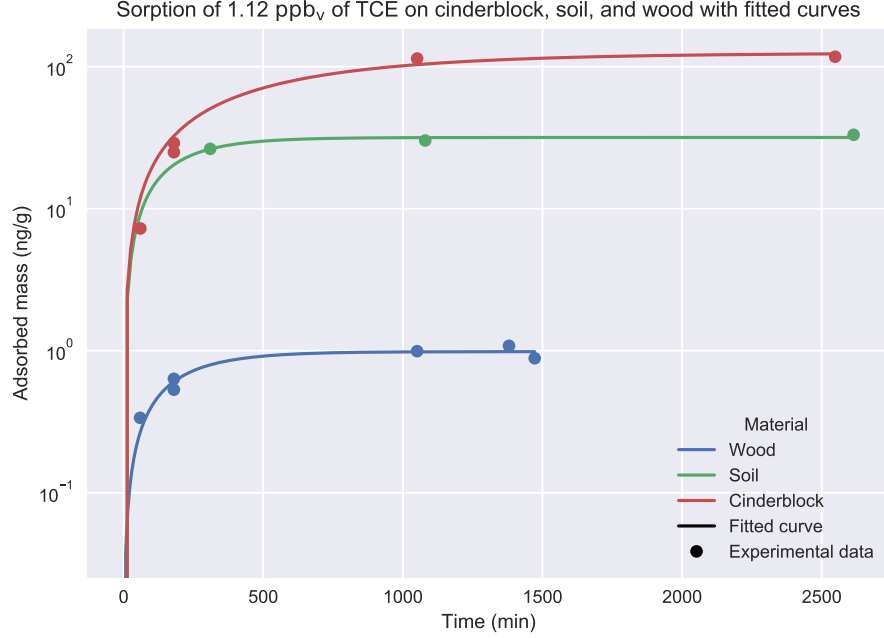


Figure 3: Experimental data of sorption of TCE onto three select materials as well as fitted sorption rates based on the kinetic model (22).

250 larger sorption capacities than wood or drywall does. We can also see by the
 251 k_2 values that soil and cinderblock sorb quickly, much faster than a material
 252 with similar sorptive capacity such as paper.

Table 2: Fitted kinetic sorption parameters based on sorption experiment data.

Material	k_1 (1/hr)	k_2 (1/hr)	K
Wood	0.32	44.90	$7.10 \cdot 10^{-3}$
Drywall	0.41	87.94	$4.65 \cdot 10^{-3}$
Carpet	0.26	58.74	$4.42 \cdot 10^{-3}$
Paper	0.04	88.37	$4.55 \cdot 10^{-4}$
Soil	0.34	2636.57	$1.30 \cdot 10^{-4}$
Cinderblock	0.10	4175.16	$2.40 \cdot 10^{-5}$

253 *3.2. Soil Sorption's Retarding Effect*

Building pressurization is a key factor in VI that influences the advective contaminant transport. The magnitude of change in response to a pressurization change is significantly influenced by a range of factors, such as soil permeability, foundation depth, or soil moisture. To demonstrate the effect that soil sorption has on contaminant soil mass transport in the VI context, we run two types transient simulation where initially the modeled structure is at a steady -5 Pa, i.e. slightly depressurized. At the start of the simulation, the building building is 1) further depressurized to -15 Pa, or 2) overpressurized to 15 Pa, and the simulation is allowed to run for 72 hours.

$$\text{Depressurization : } \Delta p_{\text{in/out}} = \begin{cases} -5, & t = 0 \text{ (hr)} \\ -15, & 0 < t \leq 72 \text{ (hr)} \end{cases} \quad (26)$$

$$\text{Overpressurization : } \Delta p_{\text{in/out}} = \begin{cases} -5, & t = 0 \text{ (hr)} \\ 15, & 0 < t \leq 72 \text{ (hr)} \end{cases} \quad (27)$$

254 For each of these cases, the simulation is run using two different soil types
 255 - sand and sandy loam. Sand is assumed here to not sorb any TCE, while
 256 for sandy loam a range of sorption isotherms are used. These range from
 257 no sorption ($K_{\text{ads}} = 0 \text{ (m}^3/\text{kg)}$) to the experimentally determined sorption
 258 isotherm ($K_{\text{ads}} = 5.28 \text{ (m}^3/\text{kg)}$) in intervals multiplicative by 10^{-2} . With the
 259 experimentally determined isotherm, we see that the ratio between sorbed
 260 concentration and soil-gas phase concentration is 7708, i.e. there is a much
 261 larger amount of sorbed contaminant. When $K_{\text{ads}} = 5.28 \cdot 10^{-4} \text{ (m}^3/\text{kg)}$ this
 262 ratio is roughly unity (0.77), which is good to keep in mind in the following
 263 discussion. These ranges of values can be used both to represent a soil that
 264 has a smaller sorptive capacity or a situation where the sorbed and gas phase
 265 has not quite reached equilibrium.

266 In the top panel of Figure 4, the indoor air contaminant concentration
 267 as the simulated building is undergoing the pressurization in (26) case. Here
 268 we can see that for the case when the surrounding soil consists of sand, the
 269 indoor concentration increases rapidly as the building is further pressurized.
 270 The rate of increase decreases significantly for the sandy loam cases, and
 271 progressively retards are the sorbed mass increases (K_{ads} increases).

272 The bottom left panel shows how far away the indoor air concentration (as
 273 attenuation factor) for each case is from reaching equilibrium. At the start
 274 of the simulation, the building starts with an attenuation of α_0 , which is the

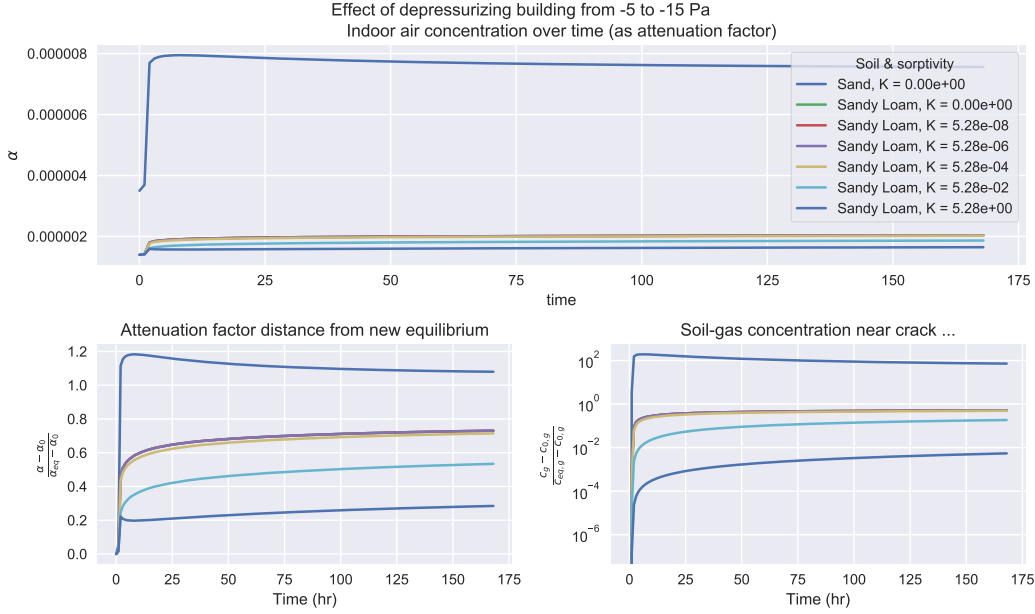


Figure 4

275 steady-state concentration when the building is pressurized with -5 Pa. As
 276 the building is further depressurized to -15 Pa, the indoor air concentration
 277 will approach a new equilibrium state α_{eq} (the result of which is from a
 278 steady-state simulation at that pressurization). By plotting $\frac{|\alpha - \alpha_0|}{|\alpha_{eq} - \alpha_0|}$ we can
 279 easily see how far away we are from the new equilibrium state, and a value
 280 of 0 represents that we are at the initial concentration, i.e. $\alpha = \alpha_0$, and a
 281 value of 1 represents $\alpha = \alpha_{eq}$.

282 This sort of analysis is applied to the bottom right panel as well, but
 283 instead of the indoor air concentration (as attenuation factor), we consider
 284 the average soil-gas concentration in a 5 cm diameter cylinder that envelop
 285 the entire perimeter crack. The choice of 5 cm is arbitrary, but helps illustrate
 286 what happens with the near-foundation-crack soil-gas concentration, changes
 287 in which allow us to better understand how the contaminant is transported
 288 into the building from the soil. The same could be done for the soil-gas
 289 velocity of course, but the rate of soil-gas velocity change is virtually the
 290 same for all of these cases, and reaches the new equilibrium velocity very
 291 quickly (much faster than the concentration) and is thus omitted from the
 292 figure.

Before discussing the role of sorption here, we can first compare the non-sorbing sand and sandy loam cases. Due to the higher permeability and lower moisture content, sand is significantly more permeable to gas flow than sandy loam (see Table 1 for permeability values). Consequently the advective transport through the foundation crack is much more significant, which is indicated by a Péclet number of around 4 versus 0.2 at a -15 Pa pressurization for sand and sandy loam respectively.

Due to the advection dominated transport mechanism in the sand case, the indoor air concentrations are temporarily elevated above the equilibrium concentration at -15 Pa, while the soil-gas concentration moves further away from equilibrium. (Note that the absolute distance from equilibrium is plotted in Figure 4 which is why at first glance one might think that the soil-gas concentration is two order of magnitude higher initially, but actually is two order of magnitude lower.) This phenomena occurs because initially more contaminants are drawn into the building from the near crack area than can be resupplied, temporarily depleting the local soil-gas contaminant concentration.

One can notice that many of the sandy loam lines overlap, and start diverging from each other when $K_{\text{ads}} = 5.28 \cdot 10^{-4}$ (m^3/kg), at the point where the ratio of sorbed and soil-gas concentration are roughly equal. We see that this divergence occurs simultaneously in the indoor air and soil-gas contaminant concentration. However, since the indoor air concentration depend on the soil-gas concentration, we know that this is where the relevant difference is.

The simple reason for this is that it is at this threshold the sorptive contribution to the retardation factor (12) starts to becomes larger than the other terms.

$$\rho_b K_H K_{\text{ads}} > \theta_w + \theta_g K_H \quad (28)$$

Thus it is at this point that the contaminant transport in the soil starts to become retarded by sorption. The physical reason for this is that the partitioning between the various phases gives a residence time as the contaminant is transported. Under VI conditions, the values of $\theta_w + \theta_g K_H$ are bounded to relatively small values, while K_{ads} can vary by orders of magnitude, making sorption potentially a very significant retarder for soil transport.

Figure 5 shows the same sort of analysis as in Figure 4 but with the building pressurization following (27). The results here are more or less the same, with the notable exception that in the sand case, the final equilibrium

329 concentration is not initially exceeded. As the building is overpressurized,
 330 the indoor contaminant are pushed out into the soil. Since the indoor air con-
 331 centration is lower than the soil-gas concentration, this is entirely expected.

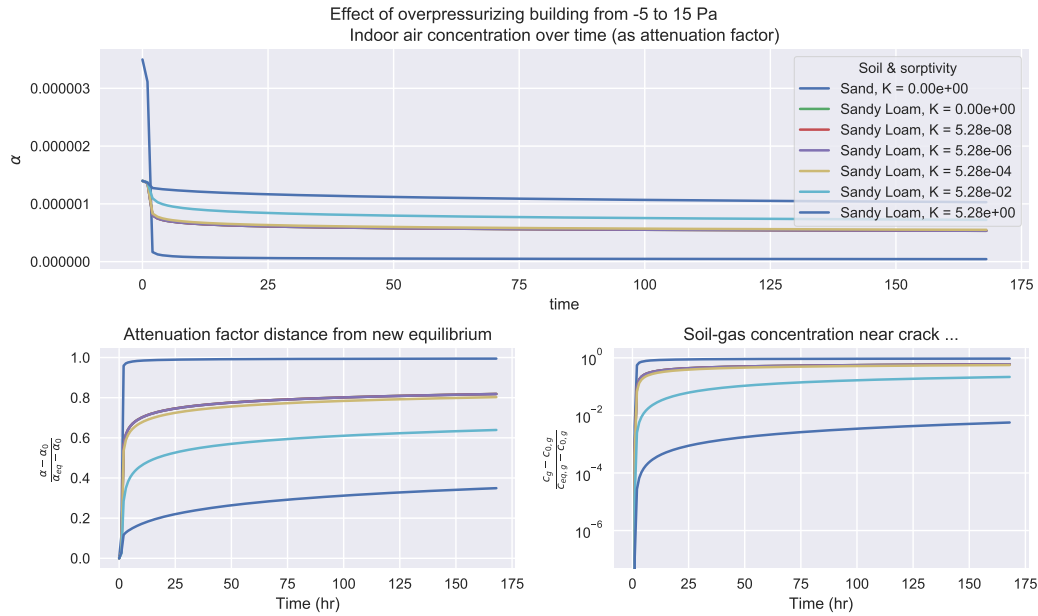


Figure 5

332 3.3. Indoor Material Sorption And Dynamics

333 3.4. Indoor Material Sorption And Mitigation

334 4. Conclusions

335 Acknowledgements

336 This project was supported by grant ES-201502 from the Strategic Envi-
 337 ronmental Research and Development Program and Environmental Security
 338 Technology Certification Program (SERDP-ESTCP).

339 Declaration of interest: none

340 References

341 [1] R. Meininghaus, L. Gunnarsen, H. N. Knudsen, Diffusion and Sorp-
 342 tion of Volatile Organic Compounds in Building Materials-Impact on

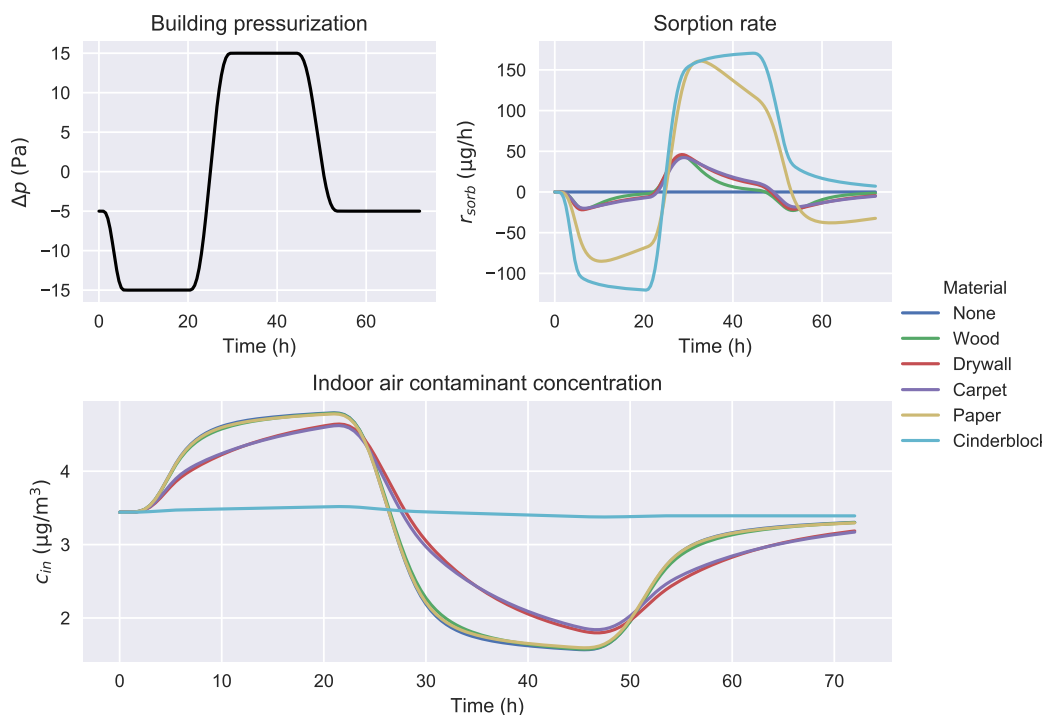


Figure 6

- Indoor Air Quality, Environ. Sci. Technol. 34 (15) (2000) 3101–3108. doi:10.1021/es991291i.
- [2] R. Meininghaus, E. Uhde, Diffusion studies of VOC mixtures in a building material, Indoor Air 12 (4) (2002) 215–222. doi:10.1034/j.1600-0668.2002.01131.x.
- [3] U.S. Environmental Protection Agency, OSWER Technical Guide for Assessing and Mitigating the Vapor Intrusion Pathway From Subsurface Vapor Sources To Indoor Air (2015).
- [4] C. Holton, Y. Guo, H. Luo, P. Dahlen, K. Gorder, E. Dettenmaier, P. C. Johnson, Long-Term Evaluation of the Controlled Pressure Method for Assessment of the Vapor Intrusion Pathway, Environ. Sci. Technol. 49 (4) (2015) 2091–2098. doi:10/f64j45.
- [5] C. C. Lutes, R. S. Truesdale, B. W. Cosky, J. H. Zimmerman, B. A. Schumacher, Comparing Vapor Intrusion Mitigation System

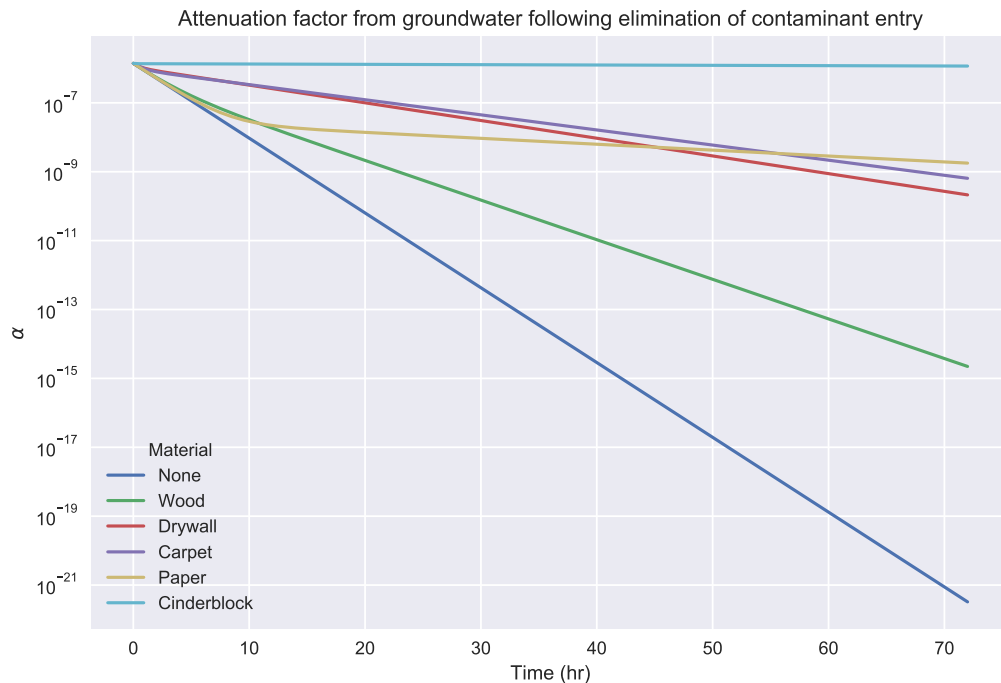


Figure 7

- 357 Performance for VOCs and Radon, Remediation 25 (4) (2015) 7–26.
 358 doi:10/gd6dfn.
- 359 [6] U.S. Environmental Protection Agency, Assessment of Mitigation Sys-
 360 tems on Vapor Intrusion: Temporal Trends, Attenuation Factors, and
 361 Contaminant Migration Routes under Mitigated And Non-mitigated
 362 Conditions (2015).
- 363 [7] T. McHugh, P. Loll, B. Eklund, Recent advances in vapor intrusion
 364 site investigations, Journal of Environmental Management 204 (2017)
 365 783–792. doi:10/gd6dgk.
- 366 [8] R. Shen, K. G. Pennell, E. M. Suuberg, A numerical investigation of
 367 vapor intrusion — The dynamic response of contaminant vapors to
 368 rainfall events, Science of The Total Environment 437 (2012) 110–120.
 369 doi:10/f4fp9s.
- 370 [9] J. G. V. Ström, Y. Guo, Y. Yao, E. M. Suuberg, Factors affect-

- 371 ing temporal variations in vapor intrusion-induced indoor air contam-
372 inant concentrations, Building and Environment 161 (2019) 106196.
373 doi:10.1016/j.buildenv.2019.106196.
- 374 [10] E. Jones, T. Oliphant, Pearu Peterson, SciPy: Open source scientific
375 tools for Python (2011).